Formation Control for CRLB-Optimal Cooperative Sensing in Low-Altitude Wireless Networks

Jun Wu, *Student Member, IEEE*, Haijia Jin, *Student Member, IEEE*, Nanchi Su, *Member, IEEE*, Jinna Li, *Senior Member, IEEE*, Haoyuan Pan, *Member, IEEE*, and Tse-Tin Chan, *Member, IEEE*

***Abstract*—Cooperative sensing with uncrewed aerial vehicles (UAVs) is a key enabler for low-altitude wireless networks (LAWNs), where sensing accuracy critically depends on the spatial configuration of the UAV formation. In this paper, we study formation design and control for CramérRao lower bound (CRLB)-optimal cooperative target sensing. We first establish a sensing performance model based on range measurements and derive the Fisher information matrix (FIM) of the target location. By adopting the A-optimality criterion, we analytically characterize the formation geometry that minimizes the CRLB of the estimation error. The optimal formation is shown to exhibit isotropic Fisher information in the horizontal plane, for which a regular polygon constitutes a symmetric CRLB-optimal geometry, with the elevation angle determined by the tradeoff between path loss and geometric diversity. Building on this result, we further develop a distributed formation control strategy that steers UAVs from arbitrary initial deployments toward the sensing-optimal configuration while maintaining formation motion and obstacle avoidance. Numerical results demonstrate that the proposed scheme consistently outperforms benchmark formations in terms of CRLB and achieves reliable convergence under practical constraints.**

***Index Terms*—Low-altitude wireless networks, cooperative sensing, CRLB, formation geometry, distributed formation control.**

I. Introduction

Low-altitude wireless networks (LAWNs) based on uncrewed aerial vehicles (UAVs) have emerged as a flexible platform for sensing, communication, and intelligence acquisition in applications such as surveillance and emergency response. Owing to their mobility and adaptive deployment capability, UAV swarms can cooperatively observe targets from multiple spatial perspectives, thereby significantly enhancing sensing accuracy compared with a single platform [1], [2].

This work was supported in part by the National Natural Science Foundation of China under Grants 62371302, 62401181, and 62673241, in part by the Shenzhen Natural Science Foundation under Grant QNXMC20250701091920028, in part by the Key Scientific and Technological Project of Education Department of Liaoning Province under Grant LJ222410148037, in part by the Xingliao Talent Program of Liaoning Province under Grant XLYC2402025, and in part by the Research Matching Grant Scheme from the Research Grants Council of Hong Kong. *(Corresponding author: Tse-Tin Chan.)*

J. Wu is with the Department of Mathematics and Information Technology, The Education University of Hong Kong, Hong Kong, China (e-mail: wjun@eduhk.hk). H. Jin is with the School of Automation and Intelligent Manufacturing, Southern University of Science and Technology, Shenzhen 518055, China (e-mail: jinhj2024@mail.sustech.edu.cn). N. Su is with Guangdong Provincial Key Laboratory of Aerospace Communication and Networking Technology, Harbin Institute of Technology (Shenzhen), Shenzhen 518055, China, and with the Department of Mathematics and Information Technology, The Education University of Hong Kong, Hong Kong, China (e-mail: sunanchi@hit.edu.cn). J. Li is with the School of Information and Control Engineering, Liaoning Petrochemical University, Fushun, 113001, China (e-mail: jnli@lnpu.edu.cn). H. Pan is with the College of Computer Science and Software Engineering, Shenzhen University, Shenzhen, China (e-mail: hypan@szu.edu.cn). T.-T. Chan is with the Department of Mathematics and Information Technology, The Education University of Hong Kong, Hong Kong, China (e-mail: tsetinchan@eduhk.hk).

In cooperative UAV sensing, the relative geometry among sensing nodes plays a fundamental role in determining estimation performance [3]. Even with identical sensing hardware and transmit power, different spatial formations can yield substantially different information gains due to geometric dilution and angular diversity. As a result, geometry-aware deployment has become a key issue in UAV-enabled sensing systems, particularly in LAWNs, where path-loss effects and limited onboard resources further amplify the impact of spatial configuration. A principled way to quantify sensing performance is through the Cramér-Rao lower bound (CRLB), which links the minimum achievable mean-squared error (MSE) to the Fisher information matrix (FIM). For example, [4] analytically characterized optimal sensor placement for time-of-arrival (ToA)-based localization by deriving closed-form CRLB-optimal geometries. To transition from static placement to dynamic environments, recent work has optimized UAV trajectories to minimize the CRLB for cooperative target tracking in LAWNs [5]. However, existing literature predominantly focuses on isolated sensor positioning or individual trajectory planning, leaving a gap in how multiple UAVs should cooperatively achieve and sustain a sensing-optimal geometric configuration. Furthermore, real-world sensing missions must navigate practical operational constraints, such as coordinated motion and obstacle avoidance [6]. In these complex environments, reliable sensing performance depends not only on instantaneous spatial geometry but also on the swarm's ability to dynamically converge to a targeted formation. These challenges limit the direct applicability of static placement, underscoring the critical need for formation designs and distributed control mechanisms that jointly guarantee geometric optimality, swarm coordination, and flight safety.

Motivated by the above, this paper investigates optimal sensing-oriented formation design and distributed control in LAWNs. In contrast to existing approaches, our focus is on jointly characterizing the sensing-optimal formation geometry and realizing it through distributed coordination under physical safety constraints. The main contributions of this paper are summarized as follows:

- We analytically characterize the sensing-optimal formation, showing that the CRLB is minimized when the FIM is isotropic, yielding a regular polygon geometry with a common elevation angle determined by the tradeoff between path-loss effects and geometric conditions.
- Subsequently, a distributed formation control strategy is developed to steer UAVs from arbitrary initial deployments toward the desired formation while ensuring coordinated motion and obstacle avoidance using only local neighbor information.

- Simulation results are provided to demonstrate that the proposed formation design and control strategy consistently outperform benchmark configurations in terms of CRLB and formation convergence behavior.

The rest of this paper is organized as follows. Sec. II introduces the system model, while Sec. III derives the optimal UAV formation geometry based on CRLB analysis. Sec. IV presents the distributed formation control strategy. Numerical results are provided in Sec. V, followed by conclusions in Sec. VI.

Notations: Bold lowercase and uppercase letters denote vectors and matrices, respectively. The operators $(\cdot)^{\mathsf{T}}$, $\|\cdot\|$, $\mathrm{tr}(\cdot)$, and $\otimes$ represent transpose, Euclidean norm, matrix trace, and Kronecker product, respectively. Moreover, $\mathbf{I}_n$, $\mathbf{0}$, and $\mathbf{1}_n$ denote the identity matrix, zero vector, and all-one vector of appropriate dimensions. The notation $\mathcal{N}(\boldsymbol{\mu}, \boldsymbol{\Sigma})$ denotes a Gaussian distribution with mean $\boldsymbol{\mu}$ and covariance $\boldsymbol{\Sigma}$.

II. System Model

As illustrated in Fig. 1, we consider a typical LAWN in which a formation of $M \geq 3$ UAVs cooperatively performs sensing of an unknown ground target. To ensure reliable sensing performance, the UAVs are required to maintain an optimized formation that fully exploits spatial diversity. In this work, our goal is twofold. First, the optimal formation shape is obtained by optimizing the cooperative sensing performance, followed by enforcing the UAVs to align their configurations with this target formation, starting from arbitrary initial deployments.

Without loss of generality, we consider an urban scenario in which all UAVs operate at a common prescribed altitude H, selected according to the surrounding infrastructure heights, as commonly assumed in UAV sensing and formation-control studies [5], [7]. Let $\mathcal{F}^\star$ denote the final desired sensing formation, in which the horizontal coordinates of UAV m are given by $\mathbf{q}_m^{\mathrm{e}} = [x_m^{\mathrm{e}}, y_m^{\mathrm{e}}]^\top$. Furthermore, the ground target to be sensed is located at $\mathbf{s} = [x_s, y_s]^\top \in \mathbb{R}^2$, such that the distance between the m-th UAV and the target can be expressed as

$$d_m = \sqrt{\| \mathbf{q}_m^{\mathrm{e}} - \mathbf{s} \|^2 + H^2}, \forall m. \tag{1}$$

For UAV m, the round-trip delay measurement τ_m is collected and converted into a range through $d_m = \tau_m c/2$, where c is the speed of light. The range estimates are affected by measurement noise, such that the measurement of d_m can be modeled as

$$\hat{d}_m = d_m + z_m, \forall m, \tag{2}$$

where $z_m \sim \mathcal{N}(0, \sigma_m^2)$ denotes the zero-mean additive white Gaussian noise (AWGN) with variance σ_m^2. Let $\mathbf{d} = [d_1, \ldots, d_M]^\top$ denote the distance vector. Generally, the measurement variance σ_m^2 is inversely proportional to the signal-to-noise ratio (SNR) at the UAV, given by $\mathrm{SNR}_m = \frac{p_m G_{\mathrm{p}} h_m}{\sigma_0^2}$, where p_m is the transmit power allocated to UAV m, G_{p} is the processing gain, and σ_0^2 is the receiver noise power. Considering a two-way sensing channel, the channel power gain h_m is characterized by a quartic path-loss model, i.e., $h_m \triangleq \frac{\beta_0}{(d_m)^4}$, where $\beta_0 \triangleq \frac{G_{\mathrm{T}} G_{\mathrm{r}} \sigma_{\mathrm{rcs}} \lambda^2}{(4\pi)^3}$ represents the reference channel power gain at a unit distance. Specifically, G_{T} and

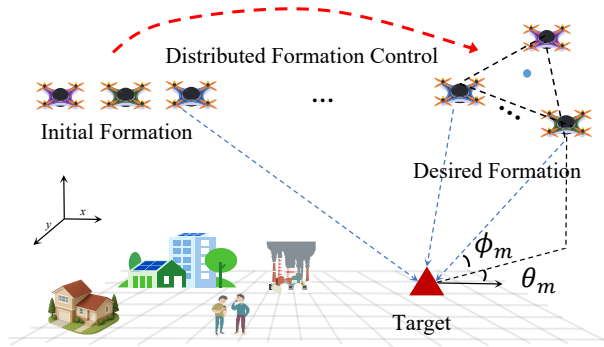

Fig. 1. The considered LAWN system where a formation is dispatched to sense the target cooperatively.

G_{r} are the transmit and receive antenna gains, respectively, σ_{rcs} is the radar cross section (RCS), and λ is the carrier wavelength. Consequently, the measurement variance can be explicitly formulated as $\sigma_m^2 = \frac{\kappa \sigma_0^2 (d_m)^4}{p_m G_{\mathrm{p}} \beta_0}$, with κ being a constant system parameter [8], [9].

During the transition of the formation toward $\mathcal{F}^\star$, the planar motions are controlled. To facilitate coordination, one UAV is selected as the formation leader, say UAV 1, while the remaining UAVs are followers. The set of UAVs is indexed by $\mathcal{M} = \{1, 2, \ldots, M\}$. At discrete time instant k, the planar position of UAV $m \in \mathcal{M}$ is denoted by $\mathbf{q}_{m,k} \in \mathbb{R}^2$. The motion of the UAV formation is modeled as the superposition of a global translational movement of the formation center and individual local adjustments that shape the formation geometry. Accordingly, the position dynamics of UAV m are described by the following first-order Gaussian Markov model [6], i.e.

$$\mathbf{q}_{m,k+1} = \mathbf{q}_{m,k} + \mathbf{u}_{m,k} + \mathbf{g}_{m,k} \Delta T + \mathbf{n}_{m,k}, \tag{3}$$

where $\mathbf{g}_{m,k} \in \mathbb{R}^2$ represents the velocity associated with the global motion at time k, $\mathbf{u}_{m,k} \in \mathbb{R}^2$ denotes the formation control input of UAV m, ΔT is the sampling interval between any two adjacent instants, and $\mathbf{n}_{m,k} \sim \mathcal{N}(\mathbf{0}, \sigma^2 \mathbf{I})$ accounts for random motion disturbance, where σ^2 denotes the disturbance variance.

III. CRLB-Optimal Formation Geometry

In this section, we derive the formation geometry $\mathcal{F}^\star$ for optimally sensing the ground target $\mathbf{s}$. In general, MSE is employed as the performance metric for unbiased estimation. To achieve MSE optimization, the A-optimality criterion, which minimizes the average estimation variance, is adopted. For ease of exposition, we assume that a prior coarse estimate of the quasi-static target's location $\mathbf{s}$ is available.[1]

To evaluate the sensing performance, we first construct the FIM of the range measurements $\mathbf{J}_{\mathbf{d}}$, such that the FIM of coordinates can be achieved via the chain rule, i.e., $\mathbf{J}_{\mathbf{s}} = \mathbf{Q}^\top \mathbf{J}_{\mathbf{d}} \mathbf{Q}$, where $\mathbf{Q} \in \mathbb{R}^{M \times 2}$ is the Jacobian matrix given by

$$\mathbf{Q} = \frac{\partial \mathbf{d}}{\partial \mathbf{s}} = \begin{bmatrix} \frac{\partial d_1}{\partial x_s} & \frac{\partial d_1}{\partial y_s} \\ \vdots & \vdots \\ \frac{\partial d_M}{\partial x_s} & \frac{\partial d_M}{\partial y_s} \end{bmatrix}. \tag{4}$$

[1]For a mobile target, the formation center can be updated according to the latest target-location estimate, while the UAVs translate with the target and maintain the derived CRLB-optimal relative geometry.

Based on (2), the likelihood function for the range measurement of the m-th UAV is given by $p(\hat{d}_m|d_m) = \frac{1}{\sqrt{2\pi\sigma_m^2}}\exp\left(-\frac{(\hat{d}_m-d_m)^2}{2\sigma_m^2}\right)$. Assuming the measurement noises among different UAVs are independent, the FIM $\mathbf{J_d} \in \mathbb{R}^{M\times M}$ is therefore a diagonal matrix. Each diagonal element $[\mathbf{J_d}]_{m,m}$ accounts for information from both the measurement mean and the variance, i.e.,

$$\begin{aligned}[\mathbf{J_d}]_{m,m} &= -\mathbb{E}\left[\frac{\partial^2 \ln p(\hat{d}_m|d_m)}{\partial d_m^2}\right] \\ &= \frac{1}{\sigma_m^2}\left(\frac{\partial d_m}{\partial d_m}\right)^2 + \frac{1}{2\sigma_m^4}\left(\frac{\partial \sigma_m^2}{\partial d_m}\right)^2.\end{aligned} \tag{5}$$

With some algebraic manipulations, we arrive at

$$[\mathbf{J_d}]_{m,m} = \frac{1}{\sigma_m^2} + \frac{1}{2\sigma_m^4}\left(\frac{4\sigma_m^2}{d_m}\right)^2 = \frac{p_m G_\mathrm{p}\beta_0}{\kappa\sigma_0^2 d_m^4} + \frac{8}{d_m^2}. \tag{6}$$

To facilitate the formation shape derivation, we have the geometric relationship between UAV m and the target as follows

$$\begin{aligned}\frac{\partial d_m}{\partial x_s} &= \frac{x_s - x_m^\mathrm{e}}{d_m} = \cos\phi_m\cos\theta_m, \\ \frac{\partial d_m}{\partial y_s} &= \frac{y_s - y_m^\mathrm{e}}{d_m} = \cos\phi_m\sin\theta_m,\end{aligned} \tag{7}$$

where $\theta_m \in [0, 2\pi]$ is the azimuth angle and $\phi_m \in (0, \pi/2)$ is the elevation angle of UAV m relative to the target. Then, the FIM for the target coordinates $\mathbf{s}$ is calculated as:

$$\mathbf{J_s} = \mathbf{Q}^\top\mathbf{J_d}\mathbf{Q} = \begin{bmatrix} J_{xx} & J_{xy} \\ J_{xy} & J_{yy}\end{bmatrix}. \tag{8}$$

The individual components of $\mathbf{J_s}$ are written by

$$\begin{aligned}J_{xx} &= \sum_{m=1}^{M} w_m\cos^2\theta_m, \quad J_{yy} = \sum_{m=1}^{M} w_m\sin^2\theta_m, \\ J_{xy} &= \sum_{m=1}^{M} w_m\sin\theta_m\cos\theta_m,\end{aligned} \tag{9}$$

with $w_m = (\frac{p_m G_\mathrm{p}\beta_0\sin^4\phi_m}{\kappa\sigma_0^2 H^4} + \frac{8\sin^2\phi_m}{H^2})\cos^2\phi_m$ due to $\sin\phi_m = H/d_m$. The A-optimality criterion minimizes $\mathrm{tr}(\mathbf{J_s}^{-1})$, i.e., $\arg\min_{\theta_m,\phi_m}\ \mathrm{tr}(\mathbf{J_s}^{-1})$. To this end, we have the following results:

Proposition 1: For any fixed weights $\{w_m\}_{m=1}^M$, the A-optimality objective satisfies

$$\mathrm{tr}\left(\mathbf{J}_s^{-1}\right) \geq \frac{4}{\sum_{m=1}^M w_m}, \tag{10}$$

where equality holds if and only if $\mathbf{J}_s = \frac{1}{2}\left(\sum_{m=1}^M w_m\right)\mathbf{I}_2$.

Proof: Let λ_1, λ_2 be the eigenvalues of the symmetric FIM $\mathbf{J_s}$. The trace of the inverse FIM is given by

$$\mathrm{tr}(\mathbf{J_s}^{-1}) = \frac{1}{\lambda_1} + \frac{1}{\lambda_2}. \tag{11}$$

According to the arithmetic-harmonic mean inequality, we have

$$\frac{1}{\lambda_1} + \frac{1}{\lambda_2} \geq \frac{4}{\lambda_1+\lambda_2} = \frac{4}{\mathrm{tr}(\mathbf{J_s})} = \frac{4}{\sum_{m=1}^M w_m}, \tag{12}$$

where equality holds if and only if $\lambda_1 = \lambda_2$, yielding $\lambda_1 = \lambda_2 = \frac{1}{2}\sum_{m=1}^M w_m$. As $\mathbf{J_s}$ is symmetric, it is orthogonally diagonalizable as $\mathbf{J_s} = \mathbf{U}\mathbf{\Lambda}\mathbf{U}^\mathsf{T}$, i.e.,

$$\mathbf{J_s} = \mathbf{U}\left(\frac{1}{2}\sum_{m=1}^M w_m\mathbf{I}_2\right)\mathbf{U}^\mathsf{T} = \frac{1}{2}\left(\sum_{m=1}^M w_m\right)\mathbf{I}_2. \tag{13}$$

This completes the proof. ■

Proposition 1 suggests that $\mathrm{tr}(\mathbf{J_s}^{-1})$ achieves minimal value $\frac{4}{\sum_{m=1}^M w_m}$ if $J_{xx} = J_{yy}$ and $J_{xy} = 0$. In other words, the determination of the optimal formation $\mathcal{F}^\star$ can be reformulated as the following optimization problem

$$\min_{\phi_m,\theta_m} \quad \frac{4}{\sum_{m=1}^M w_m} \tag{14a}$$

$$\text{s.t.} \quad \sum_{m=1}^M w_m\cos 2\theta_m = 0, \sum_{m=1}^M w_m\sin 2\theta_m = 0. \tag{14b}$$

In general, problem (14) is challenging to solve directly due to the potential coupling in (14b). However, we observe that the objective function (14a) depends solely on the elevation angles ϕ_m. [2] This allows us to determine the optimal solution via a two-step approach, i.e., solving ϕ_m that minimizes the theoretical lower bound first, followed by finding θ_m satisfying (14b). Since each UAV can independently choose its own elevation angle, the variables $\phi_1, \phi_2, \ldots, \phi_M$ are decoupled. Under the homogeneous setting with identical transmit powers and sensing parameters, all UAVs have the same weight function, yielding $\phi_1^\star = \phi_2^\star = \cdots = \phi_M^\star$. To determine the optimal $\phi_m^\star$, we set the first-order derivative of w_m with respect to ϕ_m equal to zero, yielding $\frac{dw_m}{d\phi_m} = \sin 2\phi_m D_m = 0$, where $D_m = \frac{p_m G_\mathrm{p}\beta_0}{\kappa\sigma_0^2 H^4}\left(2\sin^2\phi_m\cos^2\phi_m - \sin^4\phi_m\right) + \frac{8}{H^2}(\cos^2\phi_m - \sin^2\phi_m)$. Given that $\phi_m \in (0, \pi/2)$, it follows that $\sin 2\phi_m \neq 0$, which implies $D_m = 0$. To obtain the optimal elevation angle, define $A_m = \frac{p_m G_\mathrm{p}\beta_0}{\kappa\sigma_0^2 H^4}$, $B = \frac{8}{H^2}$, and $t_m = \tan^2\phi_m$. The condition $D_m = 0$ can then be rewritten as $(A_m + B)t_m^2 - 2A_m t_m - B = 0$. Retaining the feasible positive root yields

$$\phi_m^\star = \arctan\sqrt{\frac{A_m + \sqrt{A_m^2 + A_m B + B^2}}{A_m + B}}. \tag{15}$$

It is interesting to observe that when H is relatively small, the H^{-4} term dominates, leading $\phi_m^\star$ to asymptotically approach $\arctan(\sqrt{2}) \approx 54.74°$. At this stage, the system prioritizes maximizing the projected SNR. As H increases, the H^{-4} term decays rapidly, and the equation becomes governed by the geometric term $(\cos^2\phi_m - \sin^2\phi_m) \to 0$. Consequently, $\phi_m^\star$ converges to $45°$, shifting the priority from energy preserving to geometric robustness, i.e., $\phi_m^\star \in (45°, 54.74°)$.

Subsequently, we derive the optimal azimuth angles $\theta_m^\star$. Given that the optimal elevation angles are uniform, and thus $w_m = w^\star, \forall m$, the weights in (14b) become a common scaling factor. Consequently, the constraints for achieving the minimum CRLB reduce to the symmetry conditions

[2]Note that w_m also depends on the transmit power p_m. As this work focuses on sensing-optimal formation geometry, p_m is treated as a constant across all UAVs. Related optimizations can be found in [9]–[11].

$\sum_{m=1}^{M}\cos 2\theta_m = 0$ and $\sum_{m=1}^{M}\sin 2\theta_m = 0$, which can be compactly represented in complex form as $\sum_{m=1}^{M} e^{j2\theta_m} = 0$. This condition implies that the Fisher information must be isotropically distributed in the horizontal plane to eliminate off-diagonal correlations in the FIM. A symmetric representative solution satisfying these equations is the regular M-polygon formation, where the azimuth angles are distributed as $\theta_m^\star = \theta_0 + \frac{2\pi(m-1)}{M}$ with $\theta_0 \in [0, 2\pi)$ being an arbitrary initial rotation angle. Notice that the regular polygon is not the unique optimal solution. For example, when $M = 4$, any configuration of the form $\{\alpha, \alpha+\pi/2, \beta, \beta+\pi/2\}$ also satisfies $\sum_{m=1}^{M} e^{j2\theta_m} = 0$, yielding infinite non-regular optimal configurations. In summary, we choose the regular-polygon realization of the optimal sensing formation $\mathcal{F}^\star$, which can be geometrically characterized as an *inverted cone* with its vertex at the target's location.

IV. Distributed Formation Control

In this section, we elaborate on the distributed formation control strategy, starting from arbitrary initial formations. With $\mathcal{F}^\star$ at hand, the objective of formation control is to make the relative positions between UAVs satisfy the preset displacement vector set $\mathbb{F}$, which is defined as

$$\mathbb{F} = \left\{ \mathbf{q}_{m,k} - \mathbf{q}_{p,k} = \boldsymbol{\delta}_{pm}, \frac{\mathbf{q}_{m,k+1} - \mathbf{q}_{m,k}}{\Delta T} = \mathbf{v}^\star, \forall m, p \in \mathcal{M} \right\} \tag{16}$$

where $\boldsymbol{\delta}_{pm} \in \mathbb{R}^2$ represents the desired constant displacement of UAV m with respect to UAV p, and $\mathbf{v}^\star \in \mathbb{R}^2$ denotes the targeted global moving velocity of the entire formation.

To achieve this in a distributed manner, we first define an undirected communication graph $\mathcal{G}_f = (\mathcal{M}, \mathcal{E}, \mathcal{A})$ for the formation, where $\mathcal{M} = \{1, 2, \ldots, M\}$ is the set of UAV nodes and $\mathcal{E} \subseteq \mathcal{M} \times \mathcal{M}$ denotes the edge set, where an edge $(m, p) \in \mathcal{E}$ indicates that UAV m and p can directly exchange information. $\mathcal{A} \in \mathbb{R}^{M\times M}$ is the binary adjacency matrix with entries $a_{mp} = 1$ if $(m, p) \in \mathcal{E}$ and $a_{mp} = 0$ otherwise. According to [12], if $\mathcal{G}_f$ is connected, the desired formation $\mathcal{F}^\star$ can be uniquely characterized. In practice, communication impairments, such as packet loss and latency, may affect the connectivity of $\mathcal{G}_f$, and their impacts on distributed formation control have been extensively studied [13]–[15]. To guarantee a globally uniform velocity $\mathbf{v}^\star$ across all UAVs, we design a consensus mechanism that enables distributed velocity alignment. Assuming that only the leader has prior knowledge of $\mathbf{v}^\star$, the velocity update law for the follower UAV m at time k is given by

$$\begin{aligned} &\mathbf{v}_{m,k+1} \\ &= \mathbf{v}_{m,k} - \gamma\Big(\sum_{p\in\mathcal{M}\setminus\{1\}} a_{mp}\left(\mathbf{v}_{m,k} - \mathbf{v}_{p,k}\right) + a_{m1}\left(\mathbf{v}_{m,k} - \mathbf{v}^\star\right) \Big), \end{aligned} \tag{17}$$

where $\mathbf{v}_{m,k}$ is the desired velocity estimate of UAV m and γ is the consensus step size. If $\mathcal{G}_f$ is connected, all UAVs' velocities will asymptotically converge to $\mathbf{v}^\star$ as $k \to \infty$ [16], such that the global update can be simply written as $\mathbf{g}_{m,k} = \mathbf{v}_{m,k}$.

Subsequently, we devise the formation control input $\mathbf{u}_{m,k}$ by first constructing a decentralized cost function for UAV m

$$\begin{aligned} \mathcal{L}_m\left(\mathbb{F}, \mathbf{q}_{m,k}\right) = &\sum_{p\in\mathcal{M}} a_{mp} \left\| \mathbf{q}_{m,k} - \mathbf{q}_{p,k} - \boldsymbol{\delta}_{pm} \right\|^2 \\ &+ \left\| \frac{\mathbf{q}_{m,k+1} - \mathbf{q}_{m,k}}{\Delta T} - \mathbf{v}^\star \right\|^2, \end{aligned} \tag{18}$$

where the first term penalizes deviations from the desired relative displacements and the second term enforces alignment with the consensus-based velocity. Hence, the total cost function is given by $\mathcal{L}_{\text{tot}} = \sum_{m\in\mathcal{M}} \mathcal{L}_m\left(\mathbb{F}, \mathbf{q}_{m,k}\right)$. Motivated by (18), we design the formation-shape control input $\mathbf{u}_{m,k}$ as a distributed negative-gradient step of the displacement-error term in (18) with respect to $\mathbf{q}_{m,k}$, which yields the control policy

$$\mathbf{u}_{m,k} = -\varepsilon \sum_{p\in\mathcal{M}} a_{mp}\left(\mathbf{q}_{m,k} - \mathbf{q}_{p,k} - \boldsymbol{\delta}_{pm}\right), \tag{19}$$

with $\varepsilon > 0$ being the convergence speed tuning parameter. This displacement-based approach leverages linear closed-loop dynamics to guarantee global convergence, where only local neighbor information is required, resulting in low computational complexity and communication overhead. To prevent obstacle collisions in practice, a repulsive control component $\mathbf{u}_{m,k}^{\text{r}}$ is further integrated into the control architecture [17]. In particular, let $l_{m,k}$ be the shortest distance from UAV m to the nearest point $\mathbf{x}_{\text{near},k}$ on the obstacle surface in time instant k. Then, one can define a potential function given by

$$U_{m,k}^{\text{r}} = \frac{1}{2} E^{\text{r}} \left(\frac{1}{l_{m,k}} - \frac{1}{l_{\text{safe}}} \right)^2, \quad \text{if } l_{m,k} < l_{\text{safe}}, \tag{20}$$

where E^{r} is the repulsion gain and l_{safe} is the preset safety radius. The resulting repulsion vector $\mathbf{u}_{m,k}^{\text{r}}$ is calculated as the negative gradient of the potential function given by

$$\mathbf{u}_{m,k}^{\text{r}} = -\nabla U_{m,k}^{\text{r}} = E^{\text{r}} \left(\frac{1}{l_{m,k}} - \frac{1}{l_{\text{safe}}} \right) \frac{1}{l_{m,k}^2} \frac{\vec{\mathbf{l}}_{m,k}}{l_{m,k}}, \tag{21}$$

where $\vec{\mathbf{l}}_{m,k} = \mathbf{q}_{m,k} - \mathbf{x}_{\text{near},k}$ represents the relative displacement vector pointing from the nearest obstacle point to the UAV. For example, regarding rectangular obstacles with boundaries $[x_{\min}, x_{\max}]$ and $[y_{\min}, y_{\max}]$, the nearest point $\mathbf{x}_{\text{near},k} = [x_k, y_k]^T$ is determined by $x_k = \max(x_{\min}, \min(q_{m,k}^x, x_{\max}))$ and $y_k = \max(y_{\min}, \min(q_{m,k}^y, y_{\max}))$, with $\mathbf{q}_{m,k} = [q_{m,k}^x, q_{m,k}^y]^\top$. To accommodate formation navigation through narrow constraints, we further introduce a global scaling factor $\eta_k \in (0, 1]$ that dynamically resizes the target displacement set $\mathbb{F}$ without altering its underlying geometric topology. By incorporating both the scaling factor and the repulsive component, the total synthesized control input (19) is re-expressed as

$$\mathbf{u}_{m,k} = -\varepsilon \sum_{p\in\mathcal{M}} a_{mp}\left(\mathbf{q}_{m,k} - \mathbf{q}_{p,k} - \eta_k \boldsymbol{\delta}_{pm}\right) + \mathbf{u}_{m,k}^{\text{r}}. \tag{22}$$

Here, $\eta_k \in (0, 1]$ is adjusted according to the available obstacle clearance. It decreases when the formation approaches a narrow region and returns to one after the region is cleared. Then, the stable state evolution model can be expressed as

$\mathbf{q}_{m,k+1} = \mathbf{q}_{m,k} + \mathbf{u}_{m,k} + \mathbf{v}^\star \Delta T + \mathbf{n}_{m,k}$. We proceed to analyze the convergence of the proposed approach. To this end, we have the following proposition:

Proposition 2: Assume that the obstacle-repulsion input is inactive, i.e., $\mathbf{u}^{\mathrm{r}}_{m,k} = \mathbf{0}$, the formation scaling factor satisfies $\eta_k = 1$, and the velocity-consensus process has reached $\mathbf{g}_{m,k} = \mathbf{v}^\star$. In the absence of motion disturbances, if the undirected communication graph $\mathcal{G}_f$ is connected, the distributed control law (19) asymptotically achieves the desired formation geometry provided that

$$0 < \varepsilon < \frac{2}{\lambda_{\max}(\mathbf{L})}, \tag{23}$$

where $\mathbf{L}$ is the Laplacian matrix associated with $\mathcal{G}_f$.

Proof: Let $\mathbf{r}_m \in \mathbb{R}^2$ denote the desired position offset of UAV m relative to the formation center. The desired displacement of UAV m relative to UAV p is therefore $\boldsymbol{\delta}_{pm} = \mathbf{r}_m - \mathbf{r}_p$. Define the local state error in the moving reference frame as $\mathbf{e}_{m,k} = \mathbf{q}_{m,k} - k\Delta T \mathbf{v}^\star - \mathbf{r}_m$. It follows that

$$\mathbf{q}_{m,k} - \mathbf{q}_{p,k} - \boldsymbol{\delta}_{pm} = \mathbf{e}_{m,k} - \mathbf{e}_{p,k}. \tag{24}$$

Substituting (19) into the nominal state evolution model with $\mathbf{n}_{m,k} = \mathbf{0}$ and $\mathbf{g}_{m,k} = \mathbf{v}^\star$ yields

$$\mathbf{e}_{m,k+1} = \mathbf{e}_{m,k} - \varepsilon \sum_{p \in \mathcal{M}} a_{mp} \left(\mathbf{e}_{m,k} - \mathbf{e}_{p,k} \right). \tag{25}$$

By stacking all formation errors as $\mathbf{e}_k = \left[\mathbf{e}_{1,k}^\top, \ldots, \mathbf{e}_{M,k}^\top \right]^\top$, the system-level error dynamics can be written as

$$\mathbf{e}_{k+1} = \left[(\mathbf{I}_M - \varepsilon \mathbf{L}) \otimes \mathbf{I}_2 \right] \mathbf{e}_k. \tag{26}$$

Since $\mathcal{G}_f$ is undirected and connected, $\mathbf{L}$ is positive semidefinite and has a simple zero eigenvalue $\mu_1 = 0$ associated with the eigenvector $\mathbf{1}_M$, while all remaining eigenvalues are strictly positive, i.e., $0 = \mu_1 < \mu_2 \leq \cdots \leq \mu_M = \mu_{\max}(\mathbf{L})$. The eigenvalues of the state-transition matrix $(\mathbf{I}_M - \varepsilon \mathbf{L}) \otimes \mathbf{I}_2$ associated with the disagreement modes are $1 - \varepsilon \mu_i$, $i = 2, \ldots, M$. For the disagreement errors to converge asymptotically, all eigenvalues of the state-transition matrix associated with the nonzero Laplacian modes must lie strictly inside the unit circle. Therefore, the following condition must hold

$$|1 - \varepsilon \mu_i| < 1, \qquad i = 2, \ldots, M. \tag{27}$$

Since $\mu_i > 0$ for all $i \geq 2$, the above condition is equivalent to

$$0 < \varepsilon < \frac{2}{\mu_{\max}(\mathbf{L})}. \tag{28}$$

Under this condition, all disagreement modes converge exponentially to zero, and $\mathbf{e}_k$ converges to the consensus subspace $\mathrm{span}\{\mathbf{1}_M\} \otimes \mathbb{R}^2$. Consequently, $\lim_{k\to\infty} (\mathbf{e}_{m,k} - \mathbf{e}_{p,k}) = \mathbf{0}$, which, according to the definition of $\mathbf{e}_{m,k}$, implies

$$\lim_{k\to\infty} (\mathbf{q}_{m,k} - \mathbf{q}_{p,k}) = \boldsymbol{\delta}_{pm}. \tag{29}$$

Therefore, the desired relative formation geometry is asymptotically achieved, completing the proof. ■

Note that the scaling factor changes only the desired inter-UAV distances, while the repulsive term provides local obstacle avoidance. When η_k is fixed and the repulsive term is inactive, the convergence results in Proposition 2 applies. By doing so, the control law ensures that the UAV ensemble not only converges to the desired formation from arbitrary initializations but also maintains physical safety.

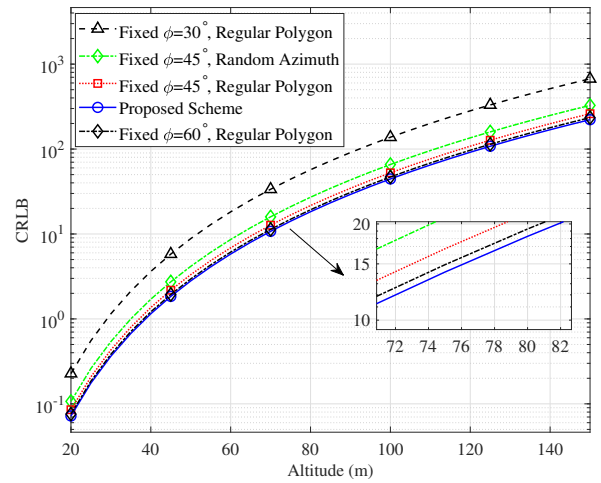

Fig. 2. The CRLB vs. flight altitudes under various formation configurations.

V. Numerical Results

In this section, we present extensive simulation results to verify the effectiveness of our proposed algorithm. We initialize $M = 6$ UAVs randomly within a rectangular area near the origin. Unless otherwise specified, the primary system parameters are summarized as follows: the flight altitude is set to $H = 20$ m, transmit power $p_m = 0.1$ W, $\forall m$, and the receiver noise power $\sigma_0^2 = -90$ dBm. The sampling interval is set to $\Delta T = 0.1$ s. The ground target is located at $\mathbf{s} = [80, 90]^\top$ m. To ensure flight safety, the obstacle avoidance radius is set to $l_{\text{safe}} = 5$ m and the tuning parameter is set to $\varepsilon = 0.01$.

Fig. 2 compares the CRLB versus UAV altitude under different formation geometries and elevation angles. The proposed scheme achieves the lowest CRLB throughout the considered altitude range. The comparison between the regular-polygon and random-azimuth formations at $\phi = 45°$ confirms the benefit of isotropic azimuth placement. Moreover, the fixed-60° formation performs consistently worse than the proposed scheme, showing that increasing the elevation angle beyond the derived upper limit does not improve localization accuracy. Although a larger elevation angle shortens the sensing distance, it reduces the horizontal geometric sensitivity of the range measurements. In contrast, the fixed-30° formation suffers from a longer sensing distance and stronger path loss. As the altitude increases, the proposed result approaches that of the fixed-45° regular polygon, which is consistent with the theoretical result that the optimal elevation angle gradually approaches 45° at higher altitudes.

In Fig. 3, we illustrate the evolution of the UAV formation in the presence of obstacles. Beginning from an arbitrary initial deployment, the UAVs first coordinate their motions to establish the desired formation structure. As the formation encounters narrow passages, the UAVs adaptively adjust their relative

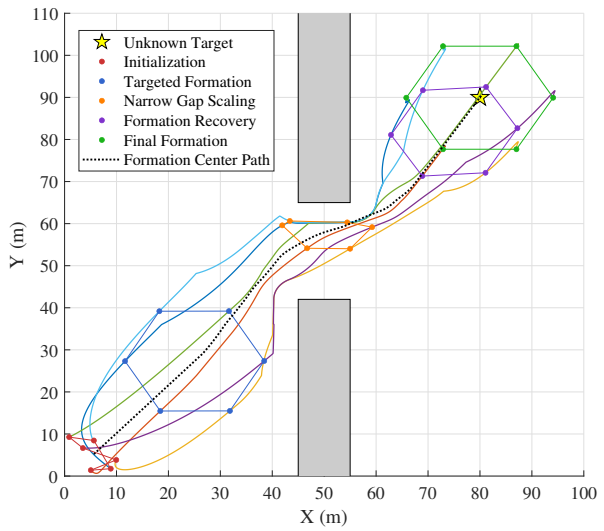

Fig. 3. The formation evolution behavior and UAV trajectory in the presence of obstacles.

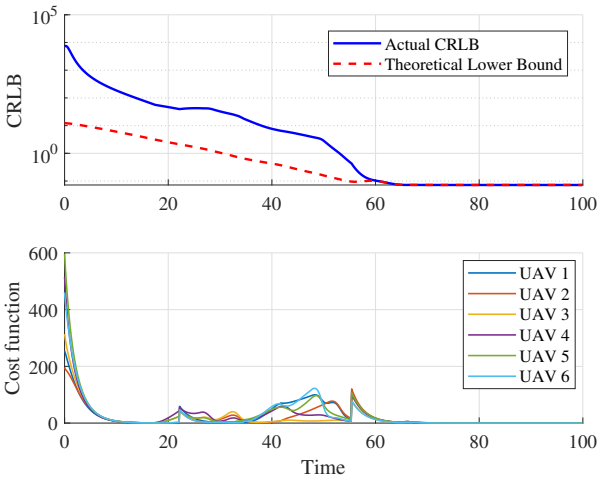

Fig. 4. The evaluation of CRLB and cost function (18).

separations, causing temporary deformation and contraction of the formation to satisfy collision-avoidance constraints. Once the obstacles are safely bypassed, the formation progressively expands and reconfigures to recover the prescribed sensing-optimal geometry $\mathcal{F}^\star$, eventually hovering over the target. This evolution process demonstrates that the proposed distributed control strategy effectively couples formation reshaping with cooperative motion.

Fig. 4 depicts the time evolution of the CRLB and the control cost (18). We observe that the CRLB decreases rapidly as the UAVs adjust their relative positions and the formation approaches the sensing-optimal geometry. As the formation converges, the CRLB stabilizes near the theoretical lower bound (12). In parallel, the control cost generally exhibits a decreasing trend as the formation stabilizes. However, a temporary increase is observed during the interval of approximately 20–60 s, corresponding to the case in which the formation encounters obstacles and undergoes deformation to satisfy collision-avoidance constraints. This deviation from the desired formation increases the control effort. It is noted that the formation gradually recovers the target configuration, and the control cost subsequently decreases and converges to a steady value.

VI. Conclusion

This paper studied CRLB-optimal formation design and distributed control for cooperative sensing in LAWNs. By analyzing range-based measurements, the Fisher information matrix for the target location was derived, and the sensing-optimal formation was analytically characterized under the A-optimality criterion, yielding a regular polygon geometry with a common elevation angle. Then, a distributed formation control strategy was developed to navigate UAVs from arbitrary initial positions toward the sensing-optimal configuration while ensuring obstacle avoidance. Extensive simulation results verified the effectiveness of the proposed design.

References

[1] W. Yuan *et al.*, "From ground to sky: Architectures, applications, and challenges shaping low-altitude wireless networks," *arXiv preprint arXiv:2506.12308*, 2025.

[2] J. Wu *et al.*, "Low-altitude wireless networks: A comprehensive survey," *China Commun.*, vol. 23, no. 3, pp. 99–141, 2026.

[3] S. Xu, "Optimal sensor placement for target localization using hybrid RSS, AOA and TOA measurements," *IEEE Commun. Lett.*, vol. 24, no. 9, pp. 1966–1970, 2020.

[4] S. Xu, Y. Ou, and X. Wu, "Optimal sensor placement for 3-D time-of-arrival target localization," *IEEE Trans. Signal Process.*, vol. 67, no. 19, pp. 5018–5031, Oct. 2019.

[5] J. Wu, W. Yuan, and L. Bai, "On the interplay between sensing and communications for UAV trajectory design," *IEEE Internet Things J.*, vol. 10, no. 23, pp. 20 383–20 395, Jun. 2023.

[6] W. Yuan, Z. Yang, L. Chen, R. Zhang, Y. Yao, Y. Cui, H. Zhang, and D. W. K. Ng, "Wireless localization and formation control with asynchronous agents," *IEEE J. Sel. Areas Commun.*, vol. 42, no. 10, pp. 2890–2904, Oct. 2024.

[7] X. Jing, F. Liu, C. Masouros, and Y. Zeng, "ISAC from the sky: UAV trajectory design for joint communication and target localization," *IEEE Trans. Wireless Commun.*, vol. 23, no. 10, pp. 12 857–12 872, 2024.

[8] F. Liu, W. Yuan, C. Masouros, and J. Yuan, "Radar-assisted predictive beamforming for vehicular links: Communication served by sensing," *IEEE Trans. Wireless Commun.*, vol. 19, no. 11, pp. 7704–7719, 2020.

[9] H. Jin *et al.*, "Co-design of sensing, communications, and control for low-altitude wireless networks," *IEEE Trans. Mobile Comput.*, vol. 24, no. 11, pp. 12 035–12 048, Nov. 2025.

[10] W. Ding *et al.*, "Multi-uav-enabled integrated sensing and communications: Joint uav placement and power control," in *2023 IEEE Globecom Workshops (GC Wkshps)*. IEEE, 2023, pp. 842–847.

[11] T. Liang, T. Zhang, B. Cao, and Q. Zhang, "Sensing, communication, and control co-design for energy-efficient UAV-aided data collection," *IEEE Wireless Commun. Lett.*, vol. 13, no. 10, pp. 2852–2856, Oct. 2024.

[12] K.-K. Oh, M.-C. Park, and H.-S. Ahn, "A survey of multi-agent formation control," *Automatica*, vol. 53, pp. 424–440, 2015.

[13] C. Viel, M. Kieffer, H. Piet-Lahanier, and S. Bertrand, "Distributed event-triggered formation control for multi-agent systems in presence of packet losses," *Automatica*, vol. 141, p. 110215, 2022.

[14] D. V. Dimarogonas, E. Frazzoli, and K. H. Johansson, "Distributed event-triggered control for multi-agent systems," *IEEE Trans. Auto.Control*, vol. 57, no. 5, pp. 1291–1297, May 2012.

[15] R. Olfati-Saber and R. M. Murray, "Consensus problems in networks of agents with switching topology and time-delays," *IEEE Trans. Auto. Control*, vol. 49, no. 9, pp. 1520–1533, Sep. 2004.

[16] W. Ren and R. W. Beard, *Distributed consensus in multi-vehicle cooperative control: theory and applications*. London, U.K.: Springer, 2008.

[17] L. A. García-Delgado *et al.*, "Repulsive function in potential field based control with algorithm for safer avoidance," *J. Intell.& Robotic Sys.*, vol. 80, no. 1, pp. 59–70, Oct. 2015.